ARTICLES
PUBLISHED ONLINE: 16 MAY 2016 | DOI: 10.1038/NMAT4645
nature materials

Exploring the origin of high optical absorption in conjugated polymers

Michelle S. Vezie[1], Sheridan Few[1], Iain Meager[2], Galatia Pieridou[3], Bernhard Dörling[4], Raja Shahid Ashraf[2], Alejandro R. Goñi[4,5], Hugo Bronstein[2,6], Iain McCulloch[2,7], Sophia C. Hayes[3], Mariano Campoy-Quiles[4]* and Jenny Nelson[1]*

The specific optical absorption of an organic semiconductor is critical to the performance of organic optoelectronic devices. For example, higher light-harvesting efficiency can lead to higher photocurrent in solar cells that are limited by sub-optimal electrical transport. Here, we compare over 40 conjugated polymers, and find that many different chemical structures share an apparent maximum in their extinction coefficients. However, a diketopyrrolopyrrole-thienothiophene copolymer shows remarkably high optical absorption at relatively low photon energies. By investigating its backbone structure and conformation with measurements and quantum chemical calculations, we find that the high optical absorption can be explained by the high persistence length of the polymer. Accordingly, we demonstrate high absorption in other polymers with high theoretical persistence length. Visible light harvesting may be enhanced in other conjugated polymers through judicious design of the structure.

Molecular electronic materials such as conjugated polymers have attracted intense interest for applications in photonics, sensing and solar energy conversion. It is well understood how optical transition energy, optical anisotropy and vibronic broadening relate to the chemical structure of the conjugated backbone and the molecular packing[1–5]. Several studies report how these properties can be controlled through the choice of structure and process route[6–9]. Some authors have addressed the broadening of spectral response using panchromatic absorbers[10] or ternary systems[11]. Absorption spectra have been analysed in terms of the relationship between spectral shape and chemical structure or conformation[12–14], and individual molecules[15] or monomers[16] with high optical extinction have been presented. However, the magnitude of the optical absorption in conjugated polymers has been less well studied and is seldom identified as a design target. The ability to tune the magnitude of absorption could strongly impact applications, for example, by enabling higher photocurrent generation in photodetectors or solar cells with imperfect charge collection, by increasing the radiative efficiency of solar cells[17], or by increasing the luminance from light emitting diodes.

Figure 1 illustrates the remarkable uniformity of extinction coefficient across a wide range of conjugated polymers, as measured using spectroscopic ellipsometry[18]. Polymers of different chemical structure, self-organizing tendency and optical gap lead to a maximum value of κ of 0.9 ± 0.1, where the complex refractive index $\eta = n + i\kappa$. Expressed in terms of the imaginary part of the dielectric function, this maximum lies around 3.9 ± 0.2 (corresponding to a linear absorption coefficient of 1.6×10^5 cm^{-1} at 700 nm). As we show below, this value lies far below their theoretical maximum absorption. Even lower values of κ are observed for low-bandgap polymers that undergo intrachain charge transfer on excitation.

In this context, we address the case of the low-bandgap polymer, thieno[3,2-b]thiophene-diketopyrrolopyrrole (DPP-TT-T). This polymer is interesting on account of the high field-effect transistor mobilities, very promising performance achieved as the donor in solar cells,[19] and high photostability[20]. Moreover the solar cell performance using this polymer has been correlated with the position of the branching point on the polymer side chains[21] and with the molecular weight of the polymer[22], but without any convincing mechanism for the trends. Here, we set out to establish the impact of these structural parameters of the polymer on its optical absorption.

From a set of polymer batches of varying molecular weight (MW) and side chain structure (Supplementary Tables 1.1 and 1.2) we select four samples for detailed study: high- (HMW) and low-MW (LMW) fractions of the polymer with dodecyl-octyl side chains branched at the second carbon (C1, $M_n = 120$ and 55 kDa) and those with tetradecyl-octyl chains branches at the fourth carbon (C3, $M_n = 84$ and 16 kDa) (see Fig. 2a,b for structures, full MW information is provided in Supplementary Section 1). When applied as the donor component in polymer:$PC_{70}BM$ solar cells of device structure glass/indium tin oxide/ZnO/polymer:fullerene(1:2)/MoO_3/Ag, (active layer thicknesses ~70–100 nm) the higher-MW polymers resulted in a substantially higher short-circuit photocurrent density, J_{sc}, leading to higher power conversion efficiencies of 8.1% and 8.5% for C1 HMW and C3 HMW, respectively, compared to the lower-MW polymers (5.8% and 4.6% for C1 LMW and C3 LMW, respectively). In contrast, the effect of the branching point on J_{sc} for polymers of similar MW is less significant (see inset values in Fig. 2e,f and Supplementary Section 2). A previous study reporting an effect of branching point on device performance had not resolved MW from side chain structure[21].

In principle, the higher J_{sc} for the high-MW fractions could result from improved electrical properties leading to higher collection

[1]Centre for Plastic Electronics and Department of Physics, Imperial College London, Prince Consort Road, London SW7 2AZ, UK. [2]Centre for Plastic Electronics and Department of Chemistry, Imperial College London, Exhibition Road, London SW7 2AZ, UK. [3]Department of Chemistry, University of Cyprus, PO Box 20537, 1678 Nicosia, Cyprus. [4]Institute of Material Science of Barcelona (ICMAB-CSIC), Campus UAB, 08193 Bellaterra, Spain. [5]ICREA, Passeig Lluís Companys 23, 08010 Barcelona, Spain. [6]Department of Chemistry, University College London, 20 Gordon Street, London WC1H 0AJ, UK. [7]SPERC, King Abdullah University of Science and Technology, Thuwal 23955-6900, Saudi Arabia. *e-mail: mcampoy@icmab.es; jenny.nelson@imperial.ac.uk

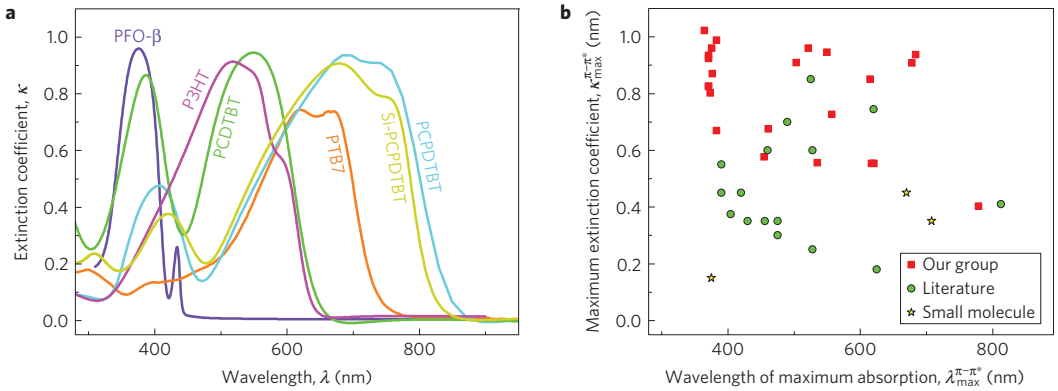

Figure 1 | Extinction coefficient κ (imaginary part of refractive index) spectra and maximum value of κ for a range of conjugated polymers. a, Spectra for a selection of conjugated polymers that have been widely studied for organic solar cells. The maximum κ lies at around 1, whereas the energetic breadth of the primary optical transition varies by <20%. **b**, Extinction coefficient maximum, $\kappa_{max}^{\pi-\pi^*}$, as a function of peak absorption wavelength for a larger set of polymers based on one or more of the following moieties: fluorene, *para*-phenylene, thiophene, cyclopentadithiophene, carbazole, isoindigo, benzodithiophene and quinoxaline. The best performing solar cell materials have maximum extinction coefficients of approximately 1. The specific materials and relevant references used to prepare this figure are tabulated in Supplementary Section 4.1.

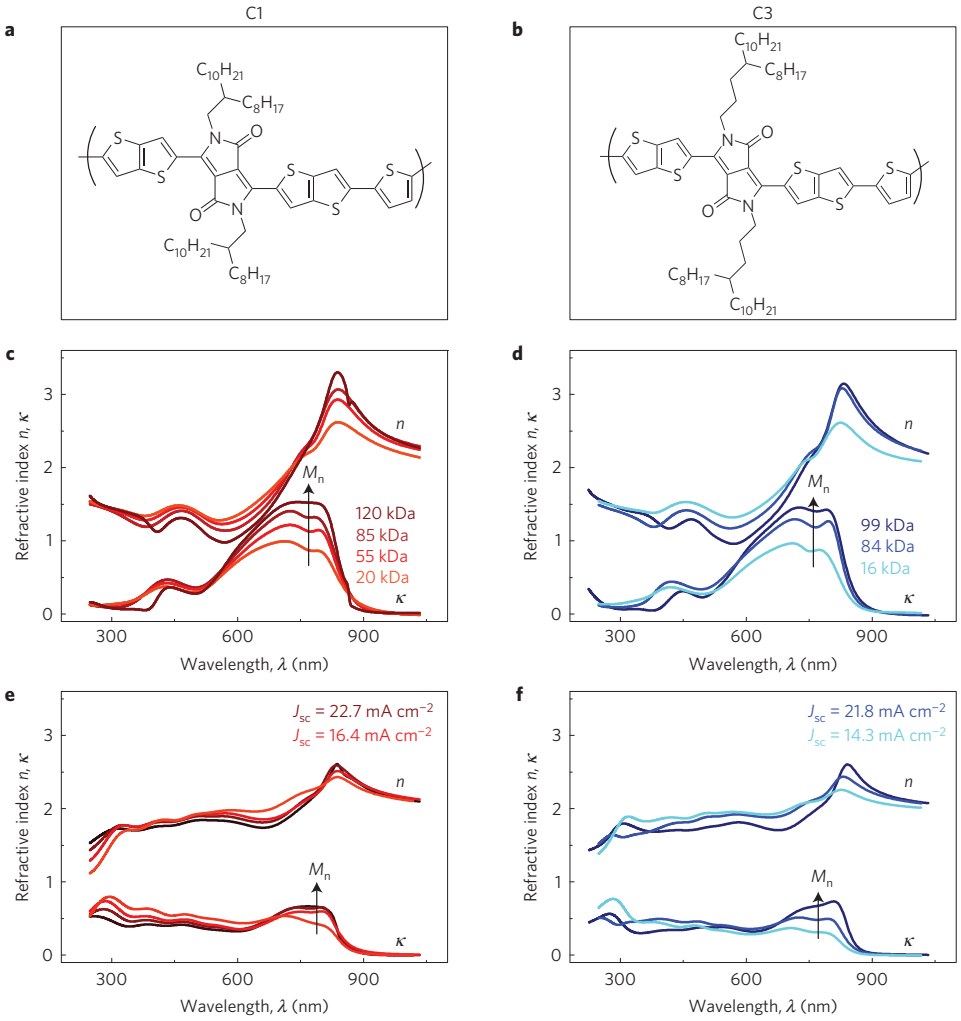

Figure 2 | Molecular structures and refractive indices of DPP-TT-T C1 and C3 polymers. a,**b**, Chemical structures of C1 and C3, respectively (synthesis details are given in ref. 21). **c**,**d**, Refractive index (n,κ) data for pristine polymer films of C1 and C3, respectively. **e**,**f**, Refractive index data for 1:2 (mass ratio) polymer:$PC_{70}BM$ blend films of C1 and C3, respectively. The C1 polymers have number-average molecular weights (M_n) of 20, 55, 85 and 120 kDa; the C3 polymers have number-average molecular weights of 16, 84 and 99 kDa. See Supplementary Tables 1.1 and 1.2 for full MW information. Also included for reference is the short-circuit current of devices made with high- and low-MW C1 (120 kDa in dark red and 55 kDa in red), and with high- and low-MW C3 (84 kDa in dark blue and 16 kDa in light blue). See Supplementary Section 1 for full MW information, and Supplementary Section 2 for full current–voltage data.

efficiency; in the present case, however, the effect cannot readily be explained either by active layer thicknesses or by differences in the charge carrier mobility or lifetime, as measured by charge extraction and transient photovoltage. Although mobilities are higher for higher-MW polymers (Supplementary Fig. 3.1), consistent with some previous reports[23,24], the mobility–lifetime products are similar for devices made from different MW fractions of either polymer (Supplementary Fig. 3.1). An alternative explanation for the observed changes in J_{sc} could be differences in optical absorption. We measured the complex dielectric function of the polymers and the corresponding blends with $PC_{70}BM$ using variable-angle spectroscopic ellipsometry. Figure 2 shows spectra for n and κ for pristine films and blend films for several MW fractions of C1 and C3. The samples with highest MW show a κ value of about 1.4 (corresponding to an absorption coefficient of $\sim 2.5 \times 10^5\ cm^{-1}$ at 700 nm), whereas the fractions with lower MW exhibit a maximum κ of about 1, similar to the polymers in Fig. 1. Note that all the samples have molecular weights in the range commonly used in organic electronics. For each material, results were confirmed using samples of different film thicknesses, different substrates, and using different ellipsometers. The trend in extinction coefficient of pristine polymer films was reproduced in measurements of blend films (Fig. 2e,f). To establish the contributions of electrical collection efficiency and optical absorption to the observed increase in J_{sc} we estimate the internal quantum efficiency (IQE) of representative devices using external quantum efficiency (EQE) measurements (Supplementary Fig. 2.2) and a transfer matrix model based on measured optical data for each layer. In each case, enhanced optical absorption is responsible for an increase in J_{sc} of 8–16% and improved IQE is responsible for a further, similar increase of 9–32%. (See Supplementary Section 2.3.) This confirms optical extinction as a major cause of higher solar cell performance.

To ascertain whether the measured extinction coefficients result from aggregation or anisotropic orientation in the solid state properties, rather than intrinsic properties of the molecules, we measured ultraviolet–visible absorption spectra of dilute solutions of the pure polymers in chloroform and 1,2-dichlorobenzene. The trend in solution is identical to that of films, with the HMW materials absorbing light more strongly at the peak absorption wavelength than the LMW materials (see Supplementary Fig. 5.1). Within the sensitivity of the ultraviolet–visible spectrometer, the pseudo molar extinction coefficient per monomer was unchanged for the range of concentrations studied ($0.25–25\ \mu g\ ml^{-1}$ in the case of C3), and the spectral shape was insensitive to dilution (Supplementary Fig. 5.3). These observations suggest that the absorption phenomena are not the result of chain aggregation in solution; however, we cannot rule out any degree of association between chains.

The results raise two important questions. First, why DPP-TT-T polymers exhibit an optical absorption strength so much higher than the values normally observed for conjugated polymers, as shown in Fig. 1, and second, how MW affects the magnitude of absorption in this polymer. We address these questions with the help of quantum chemical calculations of the oscillator strength for different materials.

The extinction coefficient κ of a molecular material can be related to the molecular orbitals through the transition dipole moment μ and the oscillator strength f. For an optical transition from state $|i\rangle$ of energy E_i to state $|j\rangle$ of energy E_j, the transition dipole moment μ_{ij} is defined as $\mu_{ij} = e\langle j|\hat{r}|i\rangle$, where $\hat{r}$ is the position operator and e is the electronic charge. The oscillator strength for the transition, assuming that the transition dipoles are oriented at random relative to the direction of the exciting electromagnetic field, is given by[25]

$$f_{ij} = \frac{2}{3}\frac{m_e}{\hbar^2 e^2}(E_j - E_i)\mu_{ij}^2 \quad (1)$$

where m_e is the mass of the electron and $\hbar$ is Planck's constant. Note that the sum of oscillator strengths for all possible transitions $i \rightarrow j$ in a system is normalized to the number N of electrons in the system according to the Thomas–Reiche–Kuhn sum rule $\sum_{i,j} f_{ij} = N$.

The linear absorption coefficient α relates to the imaginary part of the complex dielectric function $\varepsilon = \varepsilon_1 + i\varepsilon_2$ through $\alpha = (\omega/(nc))\varepsilon_2$ and also to κ, through $\alpha = ((2\omega)/c)\kappa$. Here, c represents the speed of light in vacuum, and ω represents the angular frequency of light. For a single transition, ε_2 can thus be related directly to the transition dipole moment μ_{ij}, and hence to the oscillator strength. Summing over transitions the spectrum becomes:

$$\varepsilon_2(\omega) = \frac{2\pi N_m e^2}{\varepsilon_0 m_e}\sum_{i,j}\frac{f_{ij}}{\omega}\delta(\omega - E_{ij}/\hbar) \quad (2)$$

where N_m represents the volume density of species for which f is calculated (for example, monomers) and the δ functions can be replaced by functions $D(\omega)$ representing broadened lineshapes. At this stage, we do not resolve each electronic transition into vibronic bands.

To compare the theoretical absorption strength of different conjugated polymers, we use time-dependent density functional theory (TDDFT) to calculate the oscillator strength and transition energies of the first set of excited state transitions for oligomers of $n = 1–8$ or more repeat units. We obtain a normalized oscillator strength for the dominant transition, f_1, to compare between oligomer lengths and material systems, by dividing f_{01} (oscillator strength of the first excited state) by the estimated number of π-electrons in the system, N_π. Most of the oscillator strength in the visible region resides in this first electronic transition; this can be understood in analogy with simple one-dimensional quantum systems such as the harmonic oscillator. (See Supplementary Section 6.1.)

To allow for the effect of chain conformation on optical absorption we consider two limiting cases. For all oligomers studied, the torsional potential between successive monomers has two minima: when successive monomers are rotated by approximately 180° relative to each other (here referred to as 'all-*trans*') and when monomers are oriented in the same sense (referred to as 'all-*cis*'). The '*trans*' conformation leads to more linear oligomer structures, whereas '*cis*' structures exhibit curvature of the backbone within the conjugated plane. Figure 3a shows f_1 as a function of N_π, calculated for several conjugated oligomers in the linear all-*trans* conformation. The chemical structures and optimized geometries of the materials and N_π values are listed in Supplementary Tables 6.1 and 6.2. In all systems, f_1 rises with N_π for small N_π. Although there is little experimental data on oligomer specific absorption, our results are consistent with experimental measurements of highly monodisperse oligomers of 3-hexylthiophene, which show a rising mass attenuation coefficient in solution with oligomer length up to $N \approx 25$ repeat units (see Supplementary Fig. 6.3)[26]; our calculations are also consistent with published data on absorption by polyfluorene[27] and thiophene-co-quinoxaline oligomers[28]. We attribute this rise in f_1 with N to a superlinear increase in polarizability with oligomer length, as reported for thiophene, acenes, and other elongated conjugated molecules at short lengths[29,30]. In the first excited state, μ_{01} is strongly aligned with the long axis of the oligomer, and capable of coupling strongly with a plane-polarized electromagnetic field.

Both homo-oligomers studied (fluorene and thiophene) in the all-*trans* configuration show a larger value of f_1 than any donor–acceptor structures, across the calculated range of N_π. This can be attributed in part to their high transition energy relative to the donor–acceptor copolymers (equation (1)), and does not necessarily imply high extinction at any wavelength of interest. In solar cells, for example, we seek high oscillator strength at energies where solar irradiance is high. When the effect of transition energy is removed in

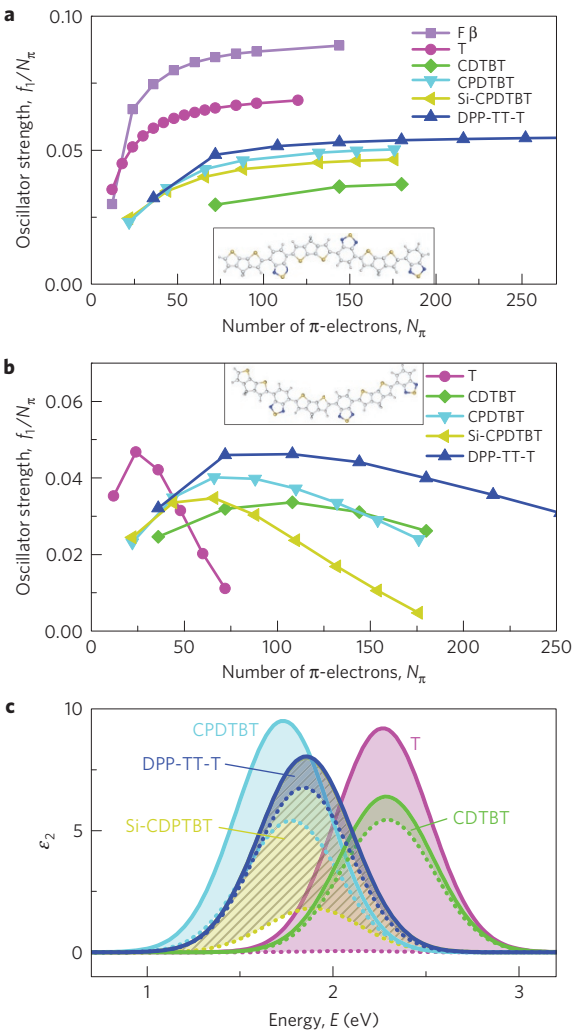

Figure 3 | Calculated oscillator strength, normalized by the number of π-electrons N_π, and corresponding ε_2 spectra. a, Normalized oscillator strength f_1 of the lowest energy transition as a function of number of π-electrons N_π, for oligomers of the corresponding polymers (see Supplementary Table 6.1 for structures) calculated in the alternating (*trans*) configuration, using TDDFT with CAM-B3LYP/6-31 g*. T refers to oligo-thiophene and F β refers to β-phase oligo-fluorene. The inset shows the calculated all-*trans* conformation of a CPDTBT oligomer. **b**, As **a** for the *cis* configuration. The inset shows the calculated all-*cis* conformation of a CPDTBT oligomer. **c**, Modelled ε_2 spectra calculated from equation (2) using calculated f_1 values for oligomers containing a similar number (around 140–160) of π-electrons. The transition is broadened with a Gaussian function of width 0.25 eV. The all-*trans* case is represented by solid lines, whereas the all-*cis* case is represented by dotted lines. The shaded area represents the range of intermediate conformations which the polymer is expected to adopt. Note that oligofluorene does not planarize, and so the *trans/cis* representation does not apply. *β*-phase oligofluorene is planar so is included in **a**, but it does not form the *cis* conformation so is omitted from **b** and **c**.

Fig. 3c by calculating ε_2 spectra for the first transition of oligomers of similar size ($N_\pi = 140$–150) in the all-*trans* conformation, then the extinction of different materials becomes comparable. Even in this representation, DPP-TT-T shows an unremarkable extinction strength. However, when variations in chain conformation are considered, the advantage of DPP-TT-T becomes evident. Figure 3b shows f_1 as a function of N_π for the same set of materials, but in the all-*cis* configuration when successive monomers are oriented alike and the backbone is curved. Now the specific oscillator strength decreases with N_π after reaching a maximum. The loss in extinction is due to the oligomer curvature, which causes μ_{01} to increase sublinearly with N_π, but the size of the effect is dependent on the chemical structure. For example, SiCPDTBT suffers a strong loss in specific extinction due to its high curvature, resulting from the large angle θ_{mon} of 44° between vectors joining successive monomer pairs, whereas DPP-TT-T with $\theta_{mon} = 27°$ and a longer monomer suffers the least (see Supplementary Fig. 6.1). Much of the lost oscillator strength is recovered in higher-lying states, but these are less useful for solar light harvesting. Allowing that, at room temperature, any conjugated polymer will sample a range of conformations, the pure *trans* and pure *cis* cases represent the limits between which the average extinction must lie. In the case of DPP-TT-T, the lower (*cis*) limit lies closer to the upper (*trans*) limit than for any other polymer studied in this evaluation.

It is important to note that curved and linear oligomers differ in their oscillator strength, but not, to a first approximation, in the transition energy, because the different conformers studied here are not strained. The effect is captured in the concept of persistence length, which can be related directly to μ, as opposed to conjugation length, which is usually related to transition energy[31,32]. DPP-TT-T offers by far the highest theoretical persistence length (λ_p) (of tens of nanometres, see Supplementary Fig. 6.8) of all materials studied here, as estimated by a simple method adapted from Flory[33] (Supplementary Section 6.8) which takes into account the thermodynamic conformational landscape. DPP-TT-T benefits from the relatively long monomer, small θ_{mon} and relative preference for *trans* alignment. The high linearity of DPP-TT-T was also noted in a computational study of polymer conformations in solution[34]. The positive correlation between persistence length and extinction coefficient has been used previously to infer conformation from extinction[35], but not in the context of designing strongly absorbing conjugated polymers. We note here that calculated values of λ_p are generally greater than values determined experimentally[35,36], suggesting that factors other than the theoretical potential energy surface may influence chain extension in practice. We also note that, although the relative depth of torsional minima influence λ_p, the steepness of the torsional potential alone is not a critical parameter.

Within this picture we can rationalize a chain length dependence of oscillator strength in DPP-TT-T. In a solution-processed polymer sample, many conformers will be present in a variety of permutations of relative monomer alignment, with chain extension lying between the all-*trans* and all-*cis* limits. The estimated persistence length reflects this distribution. The range of conformations—together with the monomer length, monomer alignment and torsional potential—results in a range of absorption strengths. In the case of DPP-TT-T, the chain curvature, and hence oscillator strength, is relatively insensitive to chain conformation (that is, all likely conformations are relatively straight), leading to an average extinction that exceeds that of all other materials studied here. For completeness, we also analysed the correlation of oscillator strength to spatial overlap of the hole and particle natural transition orbitals, and found no correlation (Supplementary Fig. 6.11).

To test the proposal that persistence length dominates optical extinction in solution we identified additional polymers with long monomers and high expected co-linearity (small θ_{mon}), namely, an indacenodithiophene-co-benzothiadiazole polymer (IDTBT)[37] and an alternative DPP-based polymer diketopyrrolopyrrole-terthiophene (DPP3T). The benefits of the high co-linearity of IDTBT are mentioned in ref. 38. IDTBT and DPP3T each have high λ_p, and show high solution absorption (Supplementary Fig. 9.2). The optical extinction in films of IDTBT and DPP3T reaches a maximum between 1.4 and 1.5 ($\alpha \approx 2.4 \times 10^5\ cm^{-1}$ at 700 nm), comparable to DPP-TT-T (Fig. 4a), and in the case of IDTBT κ increases with MW (see Supplementary Fig. 9.3). Figure 4b

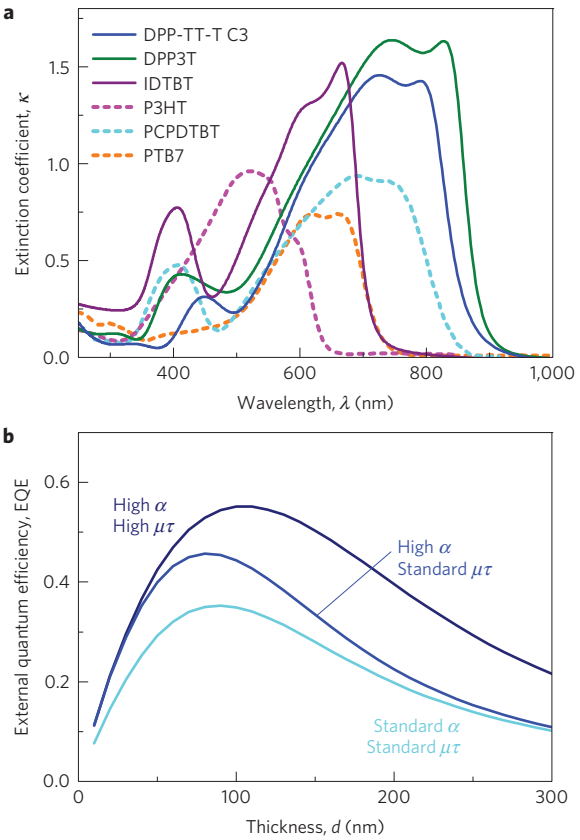

Figure 4 | Extinction coefficient of polymers with high and low theoretical persistence length (λ_p), and the effect of absorption coefficient on external quantum efficiency EQE. a, Extinction coefficient of a range of conjugated polymers: the dashed lines represent polymers which exhibit low theoretical λ_p (P3HT, PCPDTBT and PTB7), whereas solids lines represent polymers which exhibit high theoretical λ_p (DPP3T, DPP-TT-T C3 and IDTBT). The C3 polymer shown here has $M_n = 99\,kg\,mol^{-1}$. **b**, Simple model of photocurrent external quantum efficiency as a function of thickness, calculated assuming drift-dominated current and first-order carrier recombination, for the case of standard (monochromatic) absorption and standard carrier collection ($\alpha = 1.6 \times 10^5\,cm^{-1}$, $\mu\tau = 10^{-14}\,m^2\,V^{-1}$) (light blue), enhanced absorption and standard carrier collection ($\alpha = 2.4 \times 10^5\,cm^{-1}$, $\mu\tau = 10^{-14}\,m^2\,V^{-1}$) (medium blue), and enhanced absorption and enhanced carrier collection ($\alpha = 2.4 \times 10^5\,cm^{-1}$, $\mu\tau = 2 \times 10^{-14}\,m^2\,V^{-1}$) (dark blue). Maximum EQE is determined by the strength of optical absorption and by the collection efficiency. See Supplementary Section 10 for details.

illustrates the impact of such an increase in absorption on the external quantum efficiency in a collection-limited solar cell, using a simple model and a mobility–lifetime product based on the devices studied here: the increased absorption makes a higher photocurrent available. Much higher electrical quality would reduce the advantage of strong absorption in a solar cell (Supplementary Fig. 10.1a), but practical devices are at present far from that limit.

We now address the MW dependence of the extinction of DPP-TT-T. Examining the gel permeation chromatography data, we find that for both low- and high-MW fractions, the majority of the MW distributions lie at MWs beyond the point where the calculated specific extinction begins to saturate (Supplementary Fig. 1.1). Therefore, the lower specific extinction for low-MW polymer is not explained by limited polymer chain length. An alternative hypothesis is that the chains in the LMW and HMW samples are present in different distributions of conformation. This idea is supported by the higher relative strength of the second shoulder (apparent 0–1 vibronic peak) in the absorption spectrum for the LMW than the HMW sample (Fig. 2 for films, Supplementary Fig. 5.1 for solutions). It has been shown that oscillator strength is transferred from the 0–0 to higher vibronic transitions as a polymer is curved[39,40]. Interestingly, another study also showed that, as a polymer becomes more coiled, oscillator strength is lost from the lowest electronic transition and gained by higher electronic transitions[39].

To examine the vibronic structure for the DPP-TT-T samples studied here we carried out resonance Raman (RR) spectroscopy on LMW and HMW C3 polymers in solution. The intensities of RR bands are associated with structural changes on electronic excitation, and are thus directly related to the displacement between the ground and excited state potential energy surface minima along specific normal coordinates, determining in turn the shape of absorption spectra. Resonance Raman intensity analysis (RRIA) quantifies the Raman spectrum and models the RR cross-sections as a function of excitation wavelength for the most intense bands simultaneously with the absorption spectrum, thus providing the most appropriate combination of displacements and transition dipole moments to describe the optical response[41,42].

The resonance Raman spectra for the DPP-TT-T samples and the modelling approach are described in detail in the Supplementary Section 7. Primarily C=C stretching modes either belonging to the TT or the DPP unit are enhanced on excitation on the blue side of the absorption spectrum. Interestingly, the relative intensities of the bands assigned to TT and DPP units change significantly with excitation wavelength, suggesting contributions from different electronic transitions to the absorption spectrum. Moreover, our analysis showed that the RR cross-sections and absorption spectra could not be fitted simultaneously with a single dipole-allowed electronic transition; such fits greatly overestimated the RR cross-sections (Supplementary Figs 7.3 and 7.4). However, the RR cross-sections were reproduced well when a second electronic transition lying 160 meV above the first was introduced (Fig. 5a,b), inducing interference between the two transition polarizabilities, and thus reducing the RR cross-section. The second calculated electronic transition lies at around this energy, 170 meV above the first calculated transition for tetramers of DPP-TT-T. This second calculated transition is dark for linear oligomers, but moderately bright in curved (all-*cis*) oligomers with a transition dipole moment μ_{02} oriented perpendicular to the backbone (Fig. 5c). Therefore, the high-energy shoulder observed experimentally in the absorption spectrum can be assigned to the sum of two contributions, the second vibronic peak of the first electronic transition and the first vibronic peak of the second electronic transition. Both of these higher-energy contributions are expected to be stronger in curved oligomers[39,40]. Our analysis indicates that both electronic transitions, and therefore both linear (more *trans*) and curved (more *cis*) conformers, exist in both LMW and HMW samples, but the fraction of linear conformers is relatively greater in the HMW case, giving rise to the higher overall oscillator strength. We tentatively assign the higher tendency of chains to adopt linear conformation in the HMW case to the increased strength of chain–chain interactions (which will be maximized for linear chains) over the chain–solvent interactions, consistent with the lower solubility of the longer chains. The hypothesis that chain–chain interactions are more important for higher MW is consistent with the stronger effect of solvent on the absorption spectrum for the LMW than the HMW polymer (Supplementary Figs 5.2 and 7.5). The presence of the second electronic transition and conformation-dependent distribution of oscillator strength is not unique to DPP-TT-T, and is likely to occur in other materials. RRIA offers a tool to probe such phenomena.

Interestingly, we find little correlation between the push–pull character of the transition and the normalized transition dipole moment of the first transition, μ_{01}/N_π, for all the polymers we studied (see Supplementary Section 6.10). We also find little charge

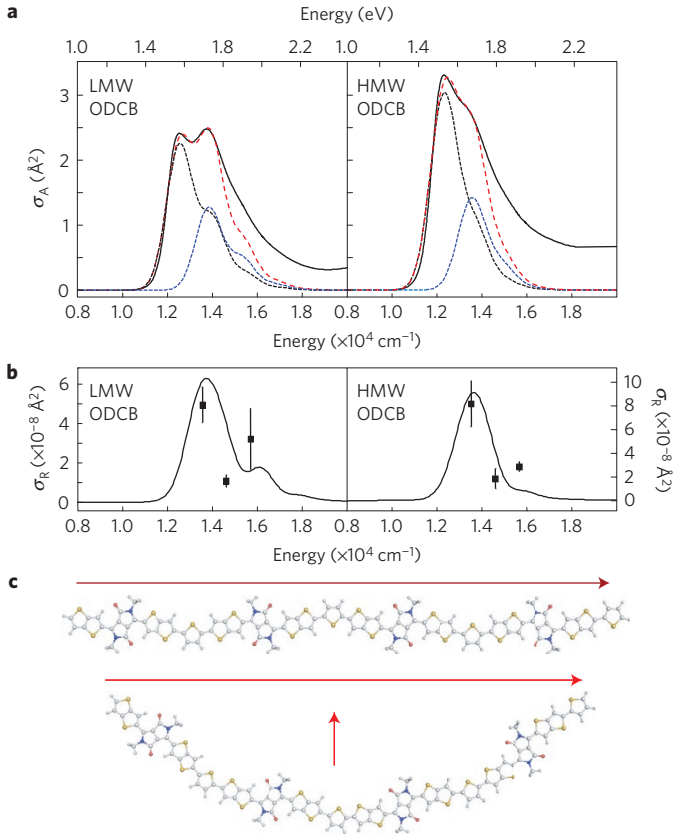

Figure 5 | Resonance Raman intensity analysis (RRIA) of dilute solutions of high- and low-MW C3 polymer in 1,2-dichlorobenzene. a, Experimental (solid black line) and calculated (dashed red line) absorption cross-sections σ_A of C3 polymers in 1,2-dichlorobenzene (ODCB). The dashed black and blue lines represent the absorption spectra for the two transitions that contribute to the overall absorption band. **b**, Corresponding experimental (points) and calculated (solid line) Raman cross-sections (σ_R) as a function of excitation wavelength for the 1,492 cm^{-1} mode of LMW and HMW C3 polymer. The error bars are the standard deviation from three measurements of the absolute cross-section of each mode at each excitation wavelength. **c**, Schematic of the direction of transition dipole moments for first two electronic transitions in linear and curved tetramers of DPP-TT-T. The top oligomer is the all-*trans* conformation, whose first electronic transition dipole is directed along the oligomer backbone, whereas the second transition is dark and is thus not shown. The bottom oligomer is the all-*cis* conformation, whose first electronic transition dipole is directed along the backbone whereas the second is directed perpendicular to the backbone. The Raman spectra can be explained by a sum of contributions from linear and curved oligomers.

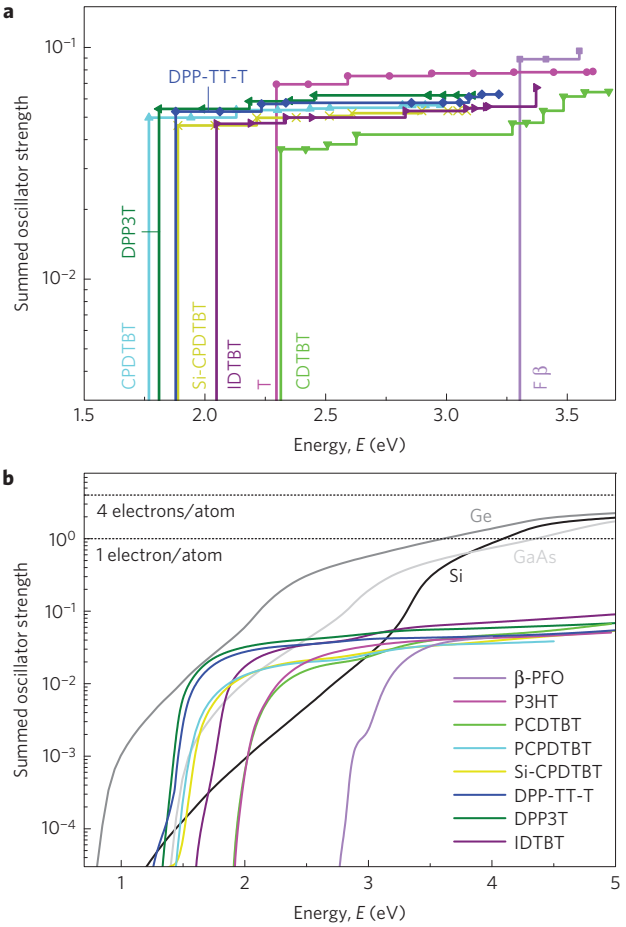

Figure 6 | Calculated and experimental summed oscillator strength per π-system electron. a, Calculated summed oscillator strength per electron in the π-system at increasing photon energies for oligomers in the all-*trans* conformation with $120 < N_\pi < 165$, using TDDFT with CAM-B3LYP/6-31g*. **b**, Experimental summed oscillator strength per π-system electron for a range of polymers. The corresponding data for key inorganic photovoltaic materials (Si, Ge and GaAs) are shown for comparison.

transfer between the thiophene block and the DPP unit on excitation to the first excited state of DPP-TT-T, consistent with a previous study[20], in contrast to the other copolymers studied. We suggest that the low excitation energy in DPP-based copolymers is due to coupling of the polymer excitation to the relatively low excitation energy and high oscillator strength of the DPP unit alone (see Supplementary Figs 6.9 and 6.10). The analysis shows that donor–acceptor character need not restrict the absorption strength of low-energy transitions.

Finally, we consider the question of the limit to absorption for a conjugated polymer. Figure 6a shows the calculated integral of oscillator strength as a function of photon energy for long oligomers ($120 < N_\pi < 165$) of a range of chemical structures. We see that the first transition contributes the majority of oscillator strength in the visible. In every case, the integrated f reaches a value much less than unity in the visible, showing that most of the available oscillator strength for the π-system must reside in higher-energy transitions outside the visible range. The low excitation energy and relatively high oscillator strength of DPP-TT-T agree well with the trend shown by the experimental results in Fig. 6b. Also shown in Fig. 6b are plots of oscillator strength per atom for the conventional semiconductors: silicon, germanium and gallium arsenide. Because the component atoms are, on average, tetravalent in these materials, the limiting oscillator strength per atom due to the valence electrons is four. The convergence of the data towards that limit shows that these inorganic materials achieve a much higher fraction of their limiting extinction within the visible region than do the organic semiconductors studied.

The examples of DPP-TT-T, DPP3T and IDTBT show that, by enhancing the coupling of a conjugated polymer to light through extended persistence length, it can be possible to pull more of the available oscillator strength into the visible region. Our studies indicate several design considerations to maximize this effect: namely, to target relatively long monomers with high co-linearity of successive monomers; to design the torsional potential to be strong and to favour an alternating (*trans*) monomer orientation; to achieve low transition energies by using components with low π–π* excitation energy and high oscillator strength, such as the DPP unit; and to exploit the competition between polymer–polymer

and polymer–solvent interactions to maximize chain extension in solution. Another strategy would be to reduce the volume fraction taken up by solubilizing side chains, although in practice this may require non-solution processing techniques. Although the absorption of a polymer in the solid state will also be affected by intermolecular interactions, there is substantial evidence that microstructure in the solid state reflects the structure in solution (for example, ref. 43). By employing these design considerations, our results indicate that polymers can be designed such that their absorption is less sensitive to conformation, thus allowing their full potential to be realized. Exploiting these aspects, along with usual considerations such as charge transport, could open the way to significant improvements in device performance, as shown here in the case of solar cells.

Methods

Methods and any associated references are available in the online version of the paper.

Received 30 July 2015; accepted 18 April 2016; published online 16 May 2016

References

1. Pope, M., Swenberg, C. E. & Pope, M. *Electronic Processes in Organic Crystals and Polymers* 2nd edn (Oxford Univ. Press, 1999).
2. Köhler, A. & Bässler, H. *Electronic Processes in Organic Semiconductors: An Introduction* (John Wiley, 2015).
3. Spano, F. C. & Silva, C. H- and J-aggregate behavior in polymeric semiconductors. *Annu. Rev. Phys. Chem.* **65,** 477–500 (2014).
4. Tian, B., Zerbi, G., Schenk, R. & Mullen, K. Optical-spectra and structure of oligomeric models of polyparaphenylenevinylene. *J. Chem. Phys.* **95,** 3191–3197 (1991).
5. Puschnig, P. *et al*. Electronic, optical, and structural properties of oligophenylene molecular crystals under high pressure: an *ab initio* investigation. *Phys. Rev. B* **67,** 235321 (2003).
6. Prest, W. M. & Luca, D. J. Origin of the optical anisotropy of solvent cast polymeric films. *J. Appl. Phys.* **50,** 6067–6071 (1979).
7. Prest, W. M. & Luca, D. J. The alignment of polymers during the solvent-coating process. *J. Appl. Phys.* **51,** 5170–5174 (1980).
8. Koynov, K. *et al*. Molecular weight dependence of chain orientation and optical constants of thin films of the conjugated polymer MEH-PPV. *Macromolecules* **39,** 8692–8698 (2006).
9. Clark, J., Chang, J. F., Spano, F. C., Friend, R. H. & Silva, C. Determining exciton bandwidth and film microstructure in polythiophene films using linear absorption spectroscopy. *Appl. Phys. Lett.* **94,** 163306 (2009).
10. Hestand, N. J. *et al*. Confirmation of the origins of panchromatic spectra in squaraine thin films targeted for organic photovoltaic devices. *J. Phys. Chem. C* **119,** 18964–18974 (2015).
11. Yao, K., Xu, Y. X., Li, F., Wang, X. F. & Zhou, L. A simple and universal method to increase light absorption in ternary blend polymer solar cells based on ladder-type polymers. *Adv. Opt. Mater.* **3,** 321–327 (2015).
12. Sjoqvist, J., Linares, M., Lindgren, M. & Norman, P. Molecular dynamics effects on luminescence properties of oligothiophene derivatives: a molecular mechanics-response theory study based on the CHARMM force field and density functional theory. *Phys. Chem. Chem. Phys.* **13,** 17532–17542 (2011).
13. Hedstrom, S., Henriksson, P., Wang, E., Andersson, M. R. & Persson, P. Light-harvesting capabilities of low band gap donor–acceptor polymers. *Phys. Chem. Chem. Phys.* **16,** 24853–24865 (2014).
14. Grimm, B., Risko, C., Azoulay, J. D., Bredas, J. L. & Bazan, G. C. Structural dependence of the optical properties of narrow bandgap semiconductors with orthogonal donor–acceptor geometries. *Chem. Sci.* **4,** 1807–1819 (2013).
15. Mishra, A. *et al*. A-D-A-type S, N-heteropentacenes: next-generation molecular donor materials for efficient vacuum-processed organic solar cells. *Adv. Mater.* **26,** 7217–7223 (2014).
16. Xu, Y. X. *et al*. Improved charge transport and absorption coefficient in indacenodithieno[3,2-b]thiophene-based ladder-type polymer leading to highly efficient polymer solar cells. *Adv. Mater.* **24,** 6356–6361 (2012).
17. Rau, U. Reciprocity relation between photovoltaic quantum efficiency and electroluminescent emission of solar cells. *Phys. Rev. B* **76,** 085303 (2007).
18. Campoy-Quiles, M., Alonso, M. I., Bradley, D. D. C. & Richter, L. J. Advanced ellipsometric characterization of conjugated polymer films. *Adv. Funct. Mater.* **24,** 2116–2134 (2014).
19. Bronstein, H. *et al*. Thieno[3,2-b]thiophene-diketopyrrolopyrrole-containing polymers for high-performance organic field-effect transistors and organic photovoltaic devices. *J. Am. Chem. Soc.* **133,** 3272–3275 (2011).
20. Wood, S. *et al*. Natures of optical absorption transitions and excitation energy dependent photostability of diketopyrrolopyrrole (DPP)-based photovoltaic copolymers. *Energy Env. Sci.* **8,** 3222–3232 (2015).
21. Meager, I. *et al*. Photocurrent enhancement from diketopyrrolopyrrole polymer solar cells through alkyl-chain branching point manipulation. *J. Am. Chem. Soc.* **135,** 11537–11540 (2013).
22. Meager, I. *et al*. Power conversion efficiency enhancement in diketopyrrolopyrrole based solar cells through polymer fractionation. *J. Mater. Chem. C* **2,** 8593–8598 (2014).
23. Kline, R. J. *et al*. Dependence of regioregular poly(3-hexylthiophene) film morphology and field-effect mobility on molecular weight. *Macromolecules* **38,** 3312–3319 (2005).
24. Chang, J.-F. *et al*. Molecular-weight dependence of interchain polaron delocalization and exciton bandwidth in high-mobility conjugated polymers. *Phys. Rev. B* **74,** 115318 (2006).
25. Fox, M. *Optical Properties of Solids* (Oxford Univ. Press, 2001).
26. Koch, F. P. *Synthesis and Physical Chemistry of a 'Monomer-up Approach'* PhD thesis, ETH Zurich (2013).
27. Schumacher, S. *et al*. Effect of exciton self-trapping and molecular conformation on photophysical properties of oligofluorenes. *J. Chem. Phys.* **131,** 154906 (2009).
28. Li, W. *et al*. One-step synthesis of precursor oligomers for organic photovoltaics—a comparative study between polymers and small molecules. *ACS Appl. Mater. Interfaces* **7,** 27106–27114 (2015).
29. van Faassen, M., de Boeij, P. L., van Leeuwen, R., Berger, J. A. & Snijders, J. G. Ultranonlocality in time-dependent current-density-functional theory: application to conjugated polymers. *Phys. Rev. Lett.* **88,** 186401 (2002).
30. Albuquerque, R. Q., Hofmann, C. C., Kohler, J. & Kohler, A. Diffusion-limited energy transfer in blends of oligofluorenes with an anthracene derivative. *J. Phys. Chem. B* **115,** 8063–8070 (2011).
31. Rossi, G., Chance, R. R. & Silbey, R. Conformational disorder in conjugated polymers. *J. Chem. Phys.* **90,** 7594–7601 (1989).
32. Soos, Z. G. & Schweizer, K. S. Absorption-spectrum of flexible conjugated polymers—the weak-disorder limit. *Chem. Phys. Lett.* **139,** 196–200 (1987).
33. Flory, P. J. *Statistical Mechanics of Chain Molecules* (Interscience Publishers, 1969).
34. Jackson, N. E. *et al*. Conformational order in aggregates of conjugated polymers. *J. Am. Chem. Soc.* **137,** 6254–6262 (2015).
35. Chung, W. J., Shibaguchi, H., Terao, K., Fujiki, M. & Naito, M. Evaluation of global conformation of polydialkylsilane using correlation between persistence length and excitonic absorption. *Macromolecules* **44,** 6568–6573 (2011).
36. Vanhee, S. *et al*. Synthesis and characterization of rigid rod poly(p-phenylenes). *Macromolecules* **29,** 5136–5142 (1996).
37. Bronstein, H. *et al*. Indacenodithiophene-co-benzothiadiazole copolymers for high performance solar cells or transistors via alkyl chain optimization. *Macromolecules* **44,** 6649–6652 (2011).
38. Venkateshvaran, D. *et al*. Approaching disorder-free transport in high-mobility conjugated polymers. *Nature* **515,** 384–388 (2014).
39. Marcus, M., Tozer, O. R. & Barford, W. Theory of optical transitions in conjugated polymers. II. Real systems. *J. Chem. Phys.* **141,** 164102 (2014).
40. Hestand, N. J. & Spano, F. C. The effect of chain bending on the photophysical properties of conjugated polymers. *J. Phys. Chem. B* **118,** 8352–8363 (2014).
41. Hayes, S. C. & Silva, C. Analysis of the excited-state absorption spectral bandshape of oligofluorenes. *J. Chem. Phys.* **132,** 214510 (2010).
42. Myers, A. B. & Mathies, R. A. in *Biological applications of Raman Spectroscopy: Resonance Raman Spectra of Polyenes and Aromatics* Vol. 2 (ed. Spiro, T. G.) 1–58 (1987).
43. van Franeker, J. J., Turbiez, M., Li, W. W., Wienk, M. M. & Janssen, R. A. J. A real-time study of the benefits of co-solvents in polymer solar cell processing. *Nature Commun.* **6,** 6229 (2015).

Acknowledgements

M.S.V. and S.F. are grateful to the Engineering and Physical Sciences Research Council (EPSRC) for a doctoral training award and a CDT studentship (EP/G037515/1), respectively. G.P. and S.C.H. acknowledge the University of Cyprus for funding through the internal grant 'ORGANIC'. B.D., A.R.G. and M.C.-Q. acknowledge financial support from the Ministerio de Economía y Competitividad of Spain through projects CSD2010–00044 (Consolider NANOTHERM), SEV-2015–0496 and MAT2012–37776 and the European Research Council through project ERC CoG648901. I.Meager., R.S.A. and I.McCulloch acknowledge support from the European Commission FP7 Project ArtESun (604397). J.N. is grateful to the Royal Society for a Wolfson Merit Award, and acknowledges financial support from EPSRC grants EP/K030671/1, EP/K029843/1 and

EP/J017361/1. The authors thank I. Alonso for performing supplementary ellipsometric measurements; we thank T. Kirchartz, J. Moore Frost, C. Müller, I. Alonso and A. Myers for helpful discussions.

Author contributions

M.S.V. coordinated the experimental work, made films, performed solution ultraviolet–visible measurements, and did electrical characterization. S.F. did the quantum chemical calculations. I.M. and H.B. made the DPP-TT-T and IDTBT polymers, respectively, under the supervision of I.McCulloch. G.P. and S.C.H. performed the RR spectroscopy measurements and subsequent analysis. B.D., A.R.G. and M.C.-Q. did the ellipsometry measurements. R.S.A. made the devices. J.N. supervised the work.

Additional information

Supplementary information is available in the online version of the paper. Reprints and permissions information is available online at www.nature.com/reprints. Correspondence and requests for materials should be addressed to M.C.-Q. or J.N.

Competing financial interests

The authors declare no competing financial interests.

Methods

The different batches and fractions of C1 and C3 polymers used in this work are listed in Supplementary Tables 1.1 and 1.2, respectively; corresponding gel permeation chromatography traces are shown in Supplementary Fig. 1.1. The polymers were all made according to the synthesis described in ref. 21. DPP-TT-T films and corresponding polymer:$PC_{70}BM$ (1:2) blends for ellipsometry were blade-coated using a Zehntner ZAA2300 blade coater at speeds ranging from 10 mm s^{-1} to 70 mm s^{-1} to vary film thickness in a range between 40 nm and 140 nm. A multi-sample investigation was performed, which typically included three film thicknesses and two different substrates (Spectrosil and silicon) for each material (five to six samples). Additional measurements were performed on selected systems using two other substrates, glass/PEDOT:PSS (30 nm) and silicon/SiO2(1,030 nm). A total of 92 samples were measured across multiple batches of the three polymers. Variable-angle spectroscopic ellipsometry (VASE) and (in some cases, photometry) data for the samples described above were acquired at three to five angles of incidence between 55 and 75 degrees using a Sopralab GES-5E rotating polarizer spectroscopic ellipsometer (SEMILAB) coupled to a charge-coupled device (CCD) detector. The data in Fig. 1 were collected by the groups at Imperial and at ICMAB over a period between 2003 and 2015. These VASE data were collected using the following ellipsometers: Semilab (Sopra) GES-5E, a RC2 instrument from J. A. Woollam Co., Inc. (USA) and a SOPRA GES-5 instrument. The standard critical point model (SCP)[44] was used to fit the data for both pristine DPP-TT-T films and corresponding blends.

Bulk heterojunction solar cells were fabricated with an inverted (ITO/ZnO/active layer/MoO_3/Ag) configuration and tested under simulated 100 mW cm^{-2} AM 1.5 G illumination in air. ITO-coated glass substrates were purchased from Psiotec and sonicated in acetone and isopropanol before being subjected to an oxygen plasma treatment. The ZnO film was then prepared by the solgel method as reported in the literature. The active layers were in all cases a polymer: $PC_{70}BM$ blend ratio of 1:2 (w/w). The active layer films were spin-coated from 15 mg ml^{-1} solutions in a chloroform:1,2-dichlorobenzene (4:1 v/v) solvent mixture. The MoO_3 and Ag electrodes for all devices in this study were evaporated in one batch, and the device area was 4.5 mm^2.

RRIA was performed on dilute solutions ($\sim 5.5 \times 10^{-5}$ M–6.5×10^{-5} M) of low- and high-MW batches of DPP-TT-T C3 (C3-16 and C3-99 respectively), prepared in chloroform (HPLC, 99.9%, Aldrich) and 1,2-dichlorobenzene (HPLC, 99.9% Aldrich), which were used as received. The exact concentration of each DPP-TT-T solution was obtained from the ultraviolet–visible spectrum (Shimadzu), using the pseudo molar extinction coefficient of DPP-TT-T at high MW (C3-99) in chloroform at 823 nm (90×10^3 l mol^{-1} cm^{-1}) and in 1,2-dichlorobenzene at 811 nm (85×10^3 l mol^{-1} cm^{-1}). The pseudo molar extinction coefficient of low-MW DPP-TT-T (C3-16) in chloroform was 70×10^3 l mol^{-1} cm^{-1} at 807 nm and in 1,2-dichlorobenzene was 65×10^3 l mol^{-1} cm^{-1} at 796 nm.

The absolute resonance Raman (RR) intensities of DPP-TT-T for the two molecular weights dissolved either in chloroform or 1,2-dichlorobenzene were measured with excitation at 636.8, 682.9 and 737.8 nm. The 682.9 and 636.8 nm excitation wavelengths employed in the RR experiments were produced by Raman shifting the second and third harmonics from a Q-switched Nd:YAG laser (PRO-230, 30 Hz, Spectra Physics) at 532 and 355 nm, respectively, in an in-house-built 1 m stainless-steel tube containing H_2 gas at 1.5 bar. The 737.8 nm excitation wavelength was produced by Raman shifting the fundamental from a Q-switched Nd:YAG laser (Lab-190, 30 Hz, Spectra Physics) at 1,064 nm, in a 1 m stainless-steel tube containing H_2 gas at 40 bar (Light Age). The excitation light was focused into a spinning cell consisting of an EPR Suprasil tube (diameter: 4 mm) attached to a rheostat-controlled motor for choice of rotation speed. Use of the spinning cell prolonged the lifetime of the samples. Modest excitation energies ($\sim$15 μJ per pulse) were employed to avoid decomposition of the sample. The Raman-scattered light was collected in a backscattering geometry and delivered to a 0.75 m focal-length Czerny–Turner spectrograph, equipped with a 1,200-grooves mm^{-1} holographic grating. The slit width was set to 100 μm, providing a 2 cm^{-1} spectral resolution at the wavelengths used in this work. The scattered light was detected by a thermoelectrically cooled 1340 × 400 pixel, back-illuminated deep depletion CCD detector (PIXIS-XB:400 BR, Princeton Instruments). Each spectrum presented here is the accumulation of 12–24 10 min spectra. Frequency calibration of the spectra was accomplished using toluene. In the calculation of the absolute RR cross-sections, the 1,002 cm^{-1} mode of toluene (9.4 M) was used as an external standard.

References

44. Campoy-Quiles, M., Nelson, J., Bradley, D. & Etchegoin, P. Dimensionality of electronic excitations in organic semiconductors: a dielectric function approach. *Phys. Rev. B* **76,** 235206 (2007).